Journal of Alloys and Compounds 750 (2018) 537–542

Contents lists available at ScienceDirect

Journal of Alloys and Compounds

journal homepage: http://www.elsevier.com/locate/jalcom

Ion transport and capacitive properties of RuO_2-SnO_2 binary films

L.A. Pocrifka [a, b, *], C.S. Ferreira [a], L. Aguilera [a], E.C. Pereira [b]

[a] University Federal of Amazonas, Department of Chemistry, Laboratory of Electrochemistry and Energy, Manaus, AM, Brazil
[b] University Federal of São Carlos, Department of Chemistry, São Carlos, SP, Brazil

ARTICLE INFO

Article history:
Received 10 October 2017
Received in revised form
27 March 2018
Accepted 3 April 2018
Available online 5 April 2018

Keywords:
Binary oxide
Ion transport
Capacitive properties
Complex capacitance

ABSTRACT

This paper reports the RuO_2-SnO_2 binary film synthesis and the influence of the SnO_2 composition increase in the ion transport and pseudocapacitive properties of RuO_2. The binary oxide was synthesized by polymeric precursors method followed deposition on a titanium substrate. XRD analysis showed the phases formed and the crystallites size of the samples. SEM allowed studying the morphology variation of the films with the addition of SnO_2. The material obtained was evaluated by electrochemical techniques in 1 M H_2SO_4 electrolyte solution. The voltammograms showed that the pseudocapacitive characteristic of the RuO_2 – SnO_2 binary film remained even for greater amount of SnO_2 in the binary mixture. The electrochemical impedance spectroscopy results are discussed in terms of complex capacitance and complex power. The relaxation time constant of the systems and capacitance values at low frequency, were determinate from complex capacitance plots.

© 2018 Elsevier B.V. All rights reserved.

1. Introduction

Electrochemical capacitors are energy storage devices which combine the power of the conventional capacitors and the energy of the batteries. These system can be used in electric vehicles, mobile phones and digital cameras [1,2]. Electrochemical capacitors can store energy in two ways, direct and indirect. In the direct form, electrochemical capacitors are constituted of large area porous materials that storage electric charge on the surface. Carbon-based materials are the most applied in direct storage [3,4]. In an indirect form, the storage occurs through quick faradaic reactions at the electrode/electrolyte interface by a mechanism known as pseudocapacitance [2]. Materials such as conductive polymers [5,6] as well as transition metal oxides are used in this case [7–9].

Ruthenium oxide has been one of the most studied as electrode material for pseudocapacitors [10–12]. This is a very attractive material due to its high specific capacitance value, wide window of potential, reversible redox reactions involving three oxidation states in 1.2 V and good thermal stability [10]. The pseudocapacitive behavior of this material depends on several factors. Among them the surface area is fundamental. Another decisive factor in the redox behavior of ruthenium oxide is the hydration degree. The reversible redox transitions in this material depend on the proton/cation exchange and electron-hopping processes. In this sense, the cations diffusion in hydrated species can occur via hopping of alkaline ions and H^+ ions between H_2O and OH^- sites, suggesting that the hydration degree improves the cations diffusion in the electrode material [10]. In spite of its great advantages, the use of RuO_2 is limited by its little abundance and consequently its high price [10,11].

One possible approach to optimize the use of RuO_2 consists of obtaining composites and/or binary oxides [13–15]. In these materials, the RuO_2 particles are homogeneously dispersed in another cheaper material, increasing the utilization of the active surface and reducing costs. For example, Chi-Chang Hu et al. [12], study the heat treatment influence in the morphological properties and crystallinity of the $RuO_x.nH_2O$ and $(Ru + Ir)O_y.mH_2O$. It was observed that the thermally treated oxides at 200 °C show a close performance to an ideal capacitor. Pusawale et al. [16] used the modified chemical deposition method to prepare films of SnO_2-RuO_2. The best result, 150 F g^{-1}, was obtained using 15% of $RuCl_3$ in the deposition bath. The work of Too et al. [17] compared the effect of deposit RuO_2 and Ru-Co binary oxide on single wall carbon nanotubes. The cobalt oxide addition improved the specific capacitance result. Chang et al. [18] prepare RuO_2-TiO_2 powder using the hydrothermal method. They observed that $Ru_{0.4}Ti_{0.6}O_2$ composition calcined at 200 °C showed the best results. RuO_2-SnO_2 films were prepared by sputtering method. Choi et al. [19] have shown that the $Sn_{0.75}Ru_{0.25}O_{1.9}$ presents the highest specific

* Corresponding author. University Federal of Amazonas, Department of Chemistry, Laboratory of Electrochemistry and Energy, Manaus, AM, Brazil.
E-mail address: pocrifka@ufam.edu.br (L.A. Pocrifka).

https://doi.org/10.1016/j.jallcom.2018.04.033
0925-8388/© 2018 Elsevier B.V. All rights reserved.

capacitance, about 88 F g^{-1}. It is clear, from those papers, that the synthesis method, synthesis experimental conditions, and molar composition used to prepare the RuO_2 drastically influence the results obtained.

Considering these aspects, in this work we carry out an investigation of the influence of RuO_2/SnO_2 ratio in the transport of ions and capacitive behavior of RuO_2. For this, RuO_2/SnO_2 were synthesized using the polymeric precursor's method. Considering that the capacitive behavior in RuO_2 is directly associated to the material hydration degree, in the present work during the process of obtaining, a thermal treatment was carried out at 400 °C. This treatment had as objective to effects minimize of the hydration degree to study more directly what is the influence of SnO_2 content on the capacitive behavior and ions transport of the RuO_2.

2. Experimental

2.1. Solution preparation

Different compositions of the RuO_2-SnO_2 electrodes were prepared using polymeric precursors method. In a beaker, citric acid (CA) was dissolved in ethylene glycol (EG), under vigorous stirring, at 60 °C. Then the two metal precursors, $RuCl_3$ e $SnCl_2$, were added to this mixture in sequence. The molar ratio of the reactants were M:CA:EG 1:3:12 where M is the molar percentage of the metal precursors %Ru:%Sn, CA is citric acid, and EG is ethylene glycol. The molar rations studied were: Ru25:Sn75, Ru50:Sn50, Ru75:Sn25 and Ru100:Sn0 which were named Ru25, Ru50, Ru75 and Ru100, respectively.

2.2. Film deposition

The solution were painted over the substrates (metallic titanium 99,7% from Ti Brazil), and treated, initially, at 110 °C for 30 min, to promote the polymerization, then at 250 °C for 20 min, to increase the adhesion of the material to substrate, and, finally, at 400 °C for 10 min, to complete burn the organic portion of the polymer. The thermal treatment of the electrodes was adopted according to other reports in the literature [20,21]. The exposed area of the electrodes was 1 cm^2. This procedure was repeated 5 times to increase the mass of active material.

2.3. Characterization

The oxide films were characterized using a Rigaku 120 X-ray diffraction (XRD) with Cu(Kα) (λ = 1,54056 Å) and the data acquisition was made in the range $2\theta = 20°$ - 70°. The sample morphology was analyzed using Scanning Electron Microscopy (SEM), ZEISS model 940a equipment. Cyclic voltammetry, galvanostatic charge-discharge and electrochemical impedance spectroscopy were used for electrochemical characterization. The experiments were carried out in a conventional three-electrode cell using an Autolab Potentiostat (PGSTAT 302 N). A saturated calomel electrode (SCE) was used as reference electrode an acid solution 1 M H_2SO_4. Cyclic voltammograms were recorded at 20 mV s^{-1} in the potential range of 0.1–1.1 V, at room temperature. The tests of electrochemical impedance spectroscopy were carried out with the aid of a frequency response analyzer module coupled to the model AUTOLAB FRA. After 300 s polarization, spectra were obtained in the frequency range of 10 mHz to 10 kHz which an alternating disturbance 10 mV peak to peak was applied.

3. Results and discussion

3.1. Structural and morphological study

Fig. 1 shows the XRD pattern of the thin films deposited on the titanium substrate. The main diffraction peaks for tin oxide are centered 2θ values at 26.7°, 34.0°, 52.0°, 54.7°, 61.9°, 64.7° and 66.0° and are in agreement with standard spectrum for SnO_2 (JCPDS 41-1445). For the ruthenium oxide, the diffraction peaks are centered 2θ values at 28.0°, 35.1° and 52.9° also in agreement with standard spectrum for RuO_2 (JCPDS 40-1290). The crystallite size of the thin film was determined by Scherrer's equation [22]:

$$d = \frac{k\lambda}{\beta cos\theta} \quad (1)$$

where d is the crystallite size, k is a shape coefficient (assuming $k = 0.9$), λ is the X-ray wavelength (1.542 Å), β is related to the width of the half height of the Bragg angle and θ is Bragg diffraction angle. The crystallites average size calculated for the Ru100 sample was 9 nm. It was observed that with the increase of the amount of Sn in the composition of the binary oxide, an increase in the crystallites average size also occurred. The calculated values were 9.0 nm, 15.8 nm, 18.5 nm, 18.8 nm and 19.0 nm for Ru100, Ru75, Ru50, Ru25 and Sn100 respectively.

The morphology of the RuO_2-SnO_2 films was characterized using SEM measurements. Fig. 2a–d presents micrographs for different composition. SEM images reveled that, for the lowest proportion of SnO_2 in the mixture (Ru75), the formation of SnO_2 100 nm agglomerates containing rounded and irregular shapes dispersed in the RuO_2 matrix. For (Ru25), there was apparently an increase in the amount of SnO_2 agglomerates observed by the smaller spacing among then in the RuO_2 matrix. The framed figures show that, at the microscopic level, the film presents cracked structure characteristics. Of all compositions, the Ru25 was the one that presented the deepest and widest cracks. In agreement with Trasatti, such structure comes from the material mechanical stress as well as the effect of temperature quenching which occur during the sample calcination [23,24]. According to Terezo and Pereira [25], this morphology is commonly found in Dimensionally Stable Anode (DSA), electrodes with metal oxides adhered to an inert substrate.

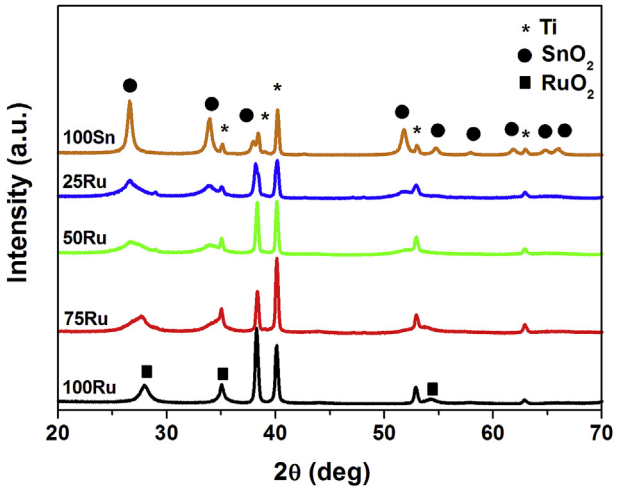

Fig. 1. XRD patterns of RuO_2-SnO_2 binary oxide thin-film electrodes at different routes.

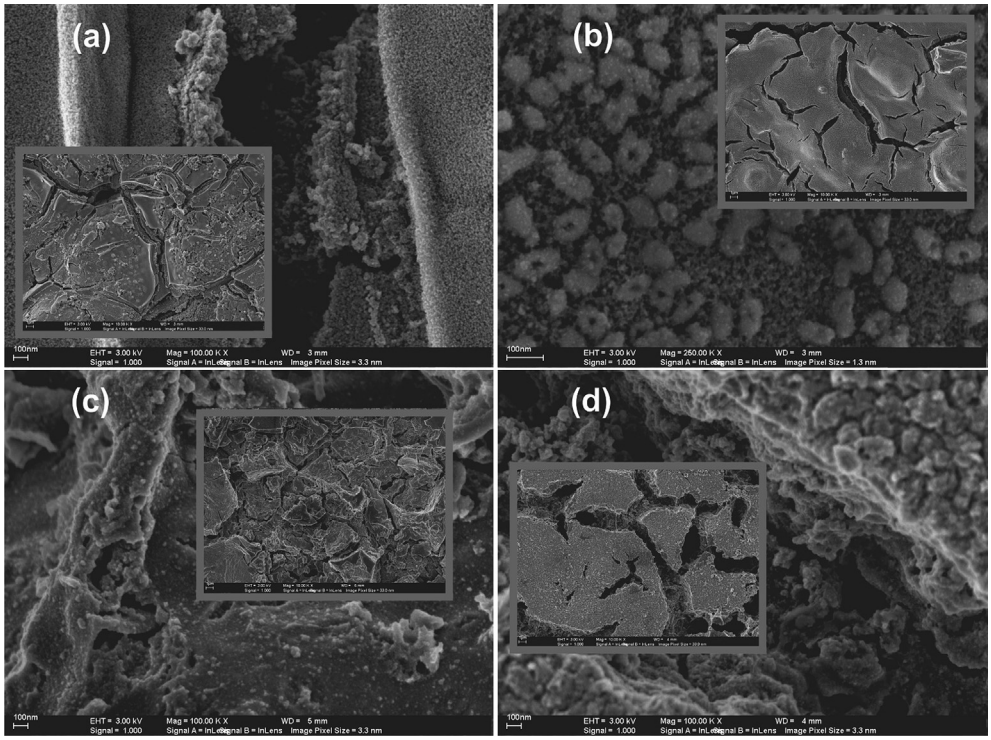

Fig. 2. SEM images of RuO_2-SnO_2 binary oxide thin-film electrodes at different routes (a) Ru100, (b) Ru75, (c) Ru50 and (d) Ru25.

3.2. Electrochemical characterization

Fig. 3 shows voltammograms of the electrodes obtained in different compositions. The profiles were normalized by the total mass of oxide deposited on the electrodes.

Analyzing Fig. 3, it was observed that current densities decrease as the SnO_2 proportion in the mixture increases. The voltammograms exhibit similar behavior to pure RuO_2, but with a lower resolution of redox processes and lower values of specific current density. In the case of pure RuO_2 film (Ru100) the wide peaks in the studied voltage range are attributed to the redox transitions Ru^{+2}/Ru^{+3}, Ru^{+3}/Ru^{+4}, and Ru^{+4}/Ru^{+6} [26]. According to literature data [27–30], the open circuit potential (E_{oc}) is an important indicator of the electrochemical behavior of the system. The typical

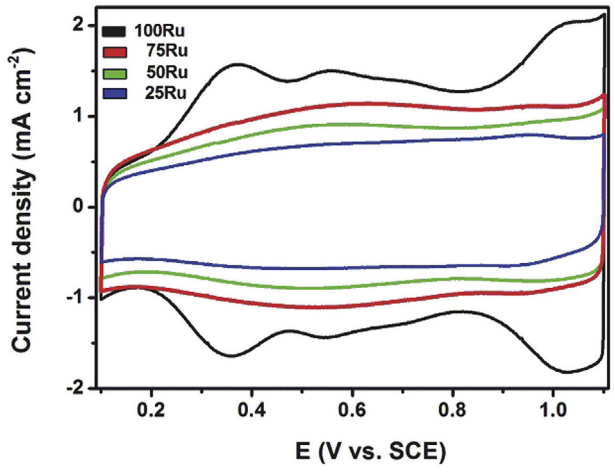

Fig. 3. Cyclic voltammograms of RuO_2-SnO_2 binary oxide thin-film at 20 mV s^{-1}.

electrochemical behavior of RuO_2 at the binary electrode is preserved when the value E_{oc} remains approximately constant at DSA systems. Table 1 shows the E_{oc} values before cyclic voltammetry study. As can be observed, the E_{oc} values are almost constant for those samples with RuO_2 composition higher than 50%. E_{oc} values decreases considerably for the sample with 25 of RuO_2. This data are in agreement with Trasatti et al. work, who proposed that the minimum amount of RuO_2 in a binary compound to guarantee RuO_2 typical behavior is 30 mol % [27,28].

Fig. 4a shows the Nyquist diagrams for different composition of RuO_2-SnO_2 binary electrodes. The material shows a typical supercapacitor behavior, where the resistance of the solution and the charge transfer resistance can be identified in the high frequencies region. Already in the high frequencies region is observed the formation of a straight line, characteristic of capacitive behavior. The R_s is the combination of the ionic and electronic resistances, the intrinsic resistance of the electrode and the contact resistance of the electrode/current collector [31] and corresponds to the initial value of the semicircle. The R_{ct} occurs due to the redox processes at the surface of the electrode [32] and corresponds to the diameter of the semicircle. Table 2 shows that the values found for R_s were close to 0.5 Ω for all compositions and the values for R_{ct} increased with the highest amount of tin added to the electrode from 0.05 to 0.44 Ω.

In the low frequencies region, for an ideal capacitor, approximately constant values of Z′ give rise to the formation of a vertical line with 90° angle [33,34]. Behavior deviations may be related with the morphological characteristics samples such as the roughness and distribution of the pores [33,34]. Fig. 4a can be seen that the samples obtained with different RuO_2/SnO_2 ratios have very little deviation from the ideal capacitor behavior, observing a great increase of the values of Z''. This fact suggests that when the electrodes are polarized in the working potential, occurs the absorption of ions in the structure without transport limitations occurring, demonstrating good accessibility of electrolyte choices

Table 1
Open circuit potential (E_{oc}) as a function of composition.

Routes	Ru_{100}	Ru_{75}	Ru_{50}	Ru_{25}
E_{oc} (V)	0.77	0.70	0.75	0.62

in binary oxides with different compositions, even for those with 75% SnO_2. The magnitude of this deviation can be calculated from the following equation [33]:

$$Z''(\omega) = \frac{1}{(jC\omega)^{\propto}} \quad with\ 0 < \propto < 1 \tag{2}$$

where Z″ is the imaginary impedance part, ω is the angular frequency, C is the capacitance and α is an adjustable constant dependent induced deflection electrode porosity and the diffusion rate. The α parameter can be obtained from the slope of *log/Z″/vs* log *f*. The values obtained for the different ratios of Ru/Sn studied were 0.9055 < 0.9018< 0.8894 < 0.8360< 0.6008 to Ru100, Ru75, Ru50, Ru 25 and Sn100 respectively.

The data of electrochemical impedance spectroscopy were transformed and analyzed by complex capacitance and power. The complex capacitance is expressed by equation [35–37]:

Table 2
Values for solution resistance (R_s) and charge transfer resistance (R_{ct}) and information about diffusion resistance.

Route	R_s (Ohm)	R_{ct} (Ohm)	Diffusional control
Ru_{100}	0.500	0.05	no
Ru_{75}	0.502	0.04	no
Ru_{50}	0.502	0.11	no
Ru_{25}	0.502	0.44	no

$$C(\omega) = C'(\omega) - jC''(\omega) \tag{3}$$

where *j* is imaginary number while the angular frequency is $\omega = 2\pi f$, $C'(\omega)$ and $C''(\omega)$ are the real and imaginary part of the complex capacitance $C(\omega)$ calculated by the following equations [35–37]:

$$C'(\omega) = -\frac{Z''(\omega)}{\omega\,|Z(\omega)|^2} \tag{4}$$

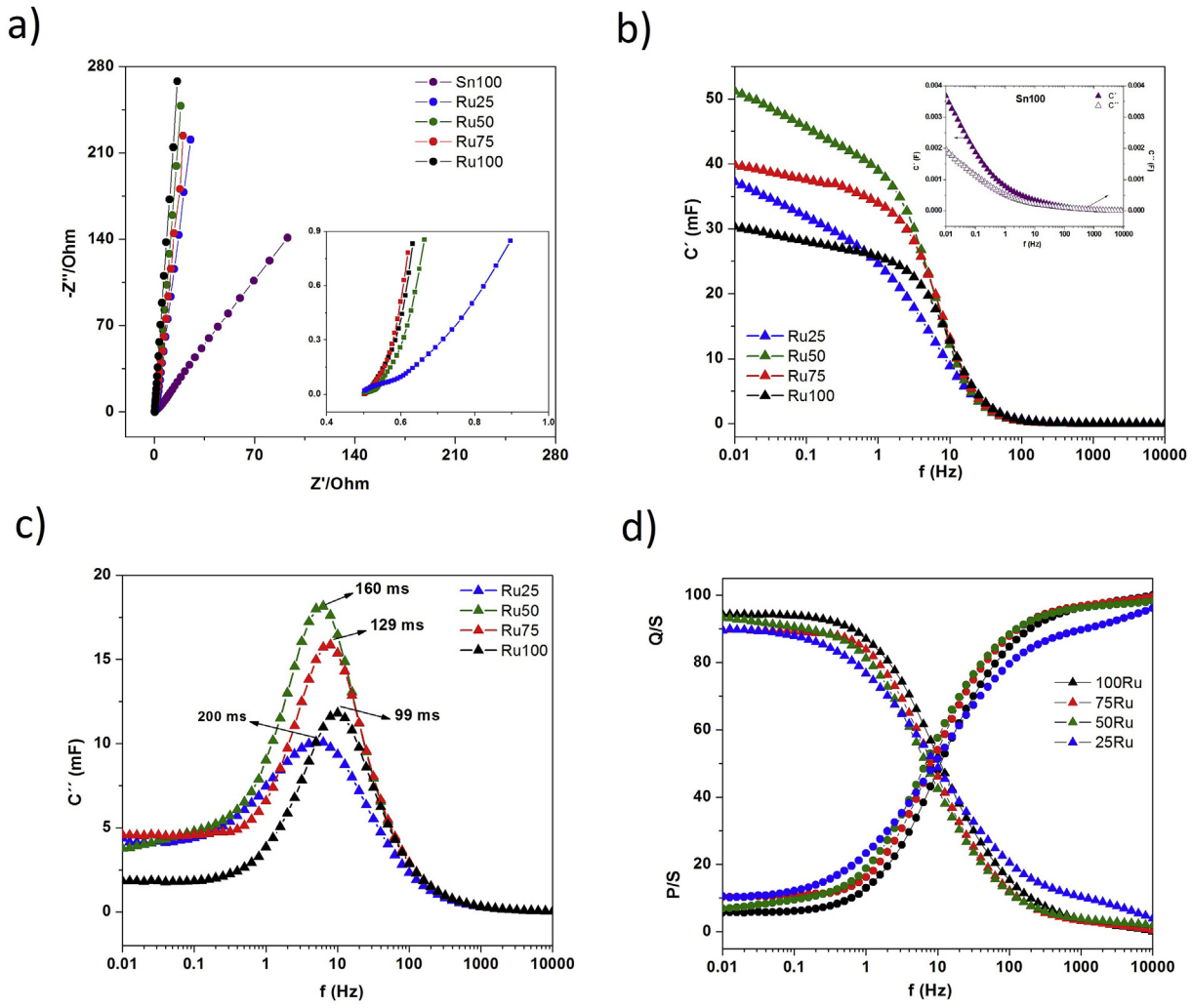

Fig. 4. (a) Electrochemical impedance spectra, (b) and (c) Real capacitance and Imaginary capacitance vs frequency and (d) Normalized power as a function of frequency for different routes.

Table 3
Electrochemical Parameters calculated from the Complex Capacitance.

	C_T (mF)	T_o (ms)
Ru_{100}	30.27	99
Ru_{75}	40.00	129
Ru_{50}	50.98	160
Ru_{25}	37.51	200
Sn_{100}	3.18	–

$$C''(\omega) = \frac{Z'(\omega)}{\omega\,|Z(\omega)|^2} \tag{5}$$

where $|Z(\omega)|$ is the module of the complex impedance calculated by $Z(\omega) = Z'(\omega) - jZ''(\omega)$.

From the graph of C′ vs f (Fig. 4b) the capacitance can be determined for the samples obtained in the different synthesis conditions. The calculated values are listed in Table 3. The C_T (mF) value is determined from the intercept with the Y axis of the graph of C′ vs f.

As can be seen the capacitance values increases with the continuous addition of Sn reaching a maximum value in the ratio Ru50: Sn50 and decreasing for the ratio of Ru25: Sn75. It is valid to note that the capacitance value for this ratio is still higher than for the sample with 100% Ru. These results suggest an increase of the electroactive sites from the intimate mixture of the Ru: Sn atoms in the binary oxides. Base on the fact that tin oxide has very low capacitance values (3.18 mF), can say that the use of the electroactive species of Ru is significantly improved with the addition of tin oxide, which may be attributable to increased defects and active sites in the material, as well as a favorable morphology for an adequate transport of ions in the structure. This facilitates that a greater number of electroactive sites are reached by the electrolyte ions and participate in the electrochemical reaction. The low capacitance values obtained, generally for all compositions, may be related to the synthesis conditions used; being that the calcination carried out at 400 °C in the process of obtaining favors the loss of hydration of the material, fact that has been identified as unfavorable to achieve high capacitance values [10,21].

Fig. 4c corresponds to the behavior of the imaginary capacitance C″ with the frequency (C″ vs f). This represents the energy dissipated irreversibly in the system and is associated with the relaxation process during the ions transport. Of the maximum capacitance at a given frequency f_o can be estimated the time constant T_o value, considered as a factor of merit in supercapacitors [34]. The T_o values are listed in Table 3. It can be seen that the lower value of T_o corresponds to the Ru100, being that in this condition the system provides the energy more quickly. In the case of Ru25, the highest value of T_o, is indicative that more time is needed to provide the power and energy of the system, which is in agreement with previous results where was shown that in this condition, a greater deviation of the ideal behavior of a supercapacitor occurs. The inset in Fig. 4b shows the behavior of the real and imaginary capacitance in samples with 100% Sn. In the studied frequencies it was not possible to determine the value of T_o for this condition, related to the poor capacitive behavior of the material. The T_o values for all the obtaining conditions, were lower than those reported by P R Deshmukh et al. [38]. Lower values of the relaxation time constant represent that the electrode has a greater ability to release energy, providing a high power density [32].

A more explicit representation of T_o can be found from the complex power model using the following equations [36,39]:

$$S(\omega) = P(\omega) + jQ(\omega) \tag{6}$$

where P is the active power and Q is the reactive power calculated by relations:

$$P(\omega) = \omega C''(\omega)\left|\Delta V_{rms}\right|^2 \tag{7}$$

$$Q(\omega) = \omega C'(\omega)\left|\Delta V_{rms}\right|^2 \tag{8}$$

where: $\Delta V_{rms} = \frac{\Delta V_{max}}{\sqrt{2}}$ and ΔV_{max} is the maximum amplitude of the applied ac perturbation.

The power dissipated was analyzed from the normalization of the active and reactive powers, $|P|/|S|$ and $|Q|/|S|$, respectively. At high frequency the electrode behaves as a resistor and the dissipated power, active power, is high. At low frequency the electrode behaves as a capacitor and the reactive power is high. When the normalized powers $|P|/|S|$ and $|Q|/|S|$ are on the same graph as a frequency function, the curves intersect at same relaxation frequency f_0 discussed for complex capacitance. Fig. 4d shows that the relaxation time constants found by complex capacitance presented approximately the same values of the complex capacitance study.

It is also possible to observe that the graphs in all the obtaining conditions have similar shapes indicating near electrochemical properties. The intercept occurs over 50% of the normalized power, being the point at which the electrodes release energy and power more efficiently [36]. From this graph it is also observed that all the samples present a capacitive behavior close to the ideal, with values of 94.32%, 89.74%, 93.15% and 89.47% for Ru100, Ru75, Ru50 and Ru25, respectively. The best results were observed for Ru100 and Ru50, confirming that even with 50% tin oxide, the binary oxide shows an excellent capacitive behavior.

4. Conclusions

The preparation of the RuO_2-SnO_2 binary electrodes, proved to be very effective in reducing the amount of Ru in terms of specific capacitance values of the films obtained. In the morphological analysis, it is observed that the surface is changed by increasing the concentration of SnO_2 in the mixture, with differences in the amounts and widths of the cracks. The decrease in the amount of ruthenium did not significantly alter the pseudocapacitive properties. Electrochemical techniques of cyclic voltammetry and electrochemical impedance spectroscopy showed similar forms for compositions analyzed. In the complex capacitance analysis, the real part (C′) increases when f decreases, indicating longer ion penetration and increased charge storage. The best result of specific capacitance was obtained for the composition Ru50 with 50.98 mF. A likely explanation for this must be related to microstructural changes that lead to changes in the density of active sites on the oxide. The relaxation time constant was used in order to study the rate capability of the electrodes.

References

[1] S.K. Chang, Z. Zainal, K.B. Tan, N.A. Yusof, W.M.D.W. Yusoff, S.R.S. Prabaharan, Nickel-cobalt oxide/activated carbon composite electrodes for electrochemical capacitors, Curr. Appl. Phys. 12 (2012) 1421–1428.
[2] B.E. Conway, Electrochemical Supercapacitors, Kluwer-Plenum Pub. Co, New York, 1999.
[3] D. Cericola, R. Kötz, Hybridization of rechargeable batteries and electrochemical capacitors: principles and limits, Electrochim. Acta 72 (2012) 1–17.
[4] J. Zhou, W. Li, Z. Zhang, X. Wu, W. Xing, S. Zhuo, Effect of cation nature of zeolite on carbon replicas and their electrochemical capacitance, Electrochim. Acta 89 (2013) 763–770.
[5] E.C. Rios, A.V. Rosário, R.M. Mello, L. Micaroni, Poly(3-methylthiophene)/MnO_2

composite electrodes as electrochemical capacitors, J. Power Sources 163 (2007) 1137–1142.
[6] E.C. Rios, A.A. Correa, F.H. Cristovan, L.A. Pocrifka, A.V. Rosário, Poly(3,4-ethylenedioxithiophene)/MnO_2 composite electrodes for electrochemical capacitors, Solid State Sci. 13 (2011) 1978–1983.
[7] M. Toupin, T. Brousse, D. Bélanger, Influence of microstructure on the charge storage properties of chemically synthesized manganese dioxide, Chem. Mater. 14 (2002) 3946–3952.
[8] V. Subramanian, H.W. Zhu, R. Vajtai, P.M. Ajayan, B.Q. Wei, Hydrothermal synthesis and pseudocapacitance properties of MnO_2 nanostructures, J. Phys. Chem. B 109 (2005) 20207–20214.
[9] T. Cottineau, M. Toupin, T. Delahaye, T. Brousse, D. Bélanger, Nanostructured transition metal oxides for aqueous hybrid electrochemical supercapacitors, Appl. Phys. A 82 (2006) 599–606.
[10] G. Wang, L. Zhang, J. Zhang, A review of electrode materials for electrochemical supercapacitors, Chem. Soc. Rev. 41 (2012) 797–828.
[11] C. Hu, Y. Huang, K. Chang, Annealing effects on the physicochemical characteristics of hydrous ruthenium and ruthenium–iridium oxides for electrochemical supercapacitors, J. Power Sources 108 (2002) 117–127.
[12] C. Wang, C. Hu, Electrochemical and textural characterization of binary Ru–Sn oxides synthesized under mild hydrothermal conditions for supercapacitors, Electrochim. Acta 50 (2005) 2573–2581.
[13] X. Zhao, B.M. Sanchez, P.J. Dobson, P.S. Grant, The role of nanomaterials in redox-based supercapacitors for next generation energy storage devices, Nanoscale 3 (2011) 839–855.
[14] Z.S. Wu, D.W. Wang, W. Ren, J. Zhao, G. Zhou, F. Li, H.M. Cheng, Anchoring hydrous RuO_2 on graphene sheets for high-performance electrochemical capacitors, Adv. Funct. Mater. 20 (2010) 3595–3602.
[15] Y.G. Wang, X.G. Zhang, Preparation and electrochemical capacitance of RuO_2/TiO_2 nanotubes composites, Electrochim. Acta 49 (2004) 1957–1962.
[16] S.N. Pusawale, P.R. Deshmukh, J.L. Gunjakar, C.D. Lokhande, SnO_2-RuO_2 composite films by chemical deposition for supercapacitor application, Mater. Chem. Phys. 139 (2013) 416–422.
[17] B.C. Kim, G.G. Wallace, Y.I. Yoon, J.M. Ko, C.O. Too, Capacitive properties of RuO_2 and Ru–Co mixed oxide deposited on single-walled carbon nanotubes for high-performance supercapacitors, Synth. Met. 159 (2009) 1389–1392.
[18] K.H. Chang, C.C. Hu, Hydrothermal synthesis of binary Ru–Ti oxides with excellent performances for supercapacitors, Electrochim. Acta 52 (2006) 1749–1757.
[19] S.H. Choi, J.S. Kim, Y.S. Yoon, Fabrication and characterization of SnO_2–RuO_2 composite anode thin film for lithium ion batteries, Electrochim. Acta 50 (2004) 547–552.
[20] L.A. Pocrifka, C. Gonçalves, P. Grossi, P.C. Colpa, E.C. Pereira, Development of RuO2–TiO2 (70–30) mol% for pH measurements, Sens. Actuators B 113 (2006) 1012–1016.
[21] L. Vázquez-Gómez, E. Horváth, J. Kristóf, A. De Battisti, Investigation of RuO2–SnO2 thin film formation by thermogravimetry–mass spectrometry and infrared emission spectroscopy, Thin Solid Films 515 (2006) 1819–1824.
[22] B.D. Cullity, Elements of X-Ray Diffraction, Addison-Wesley, New York, USA, 2014.
[23] S. Trasatti, W.E.O. Grady, Properties and applications of RuO_2–based electrodes, in: H. Gersischer, C.W. Tobias (Eds.), Advances in Electrochemistry and Electrochemical Engineering, 1991. New York.
[24] S. Trasatti, Transition metal oxide: versatile materials for electrocatalysis, in: J. Lipkowskt, P.N. Ross (Eds.), The Electrochemistry of Novel Materials, 1994. Weirheim.
[25] A.J. Terezo, E.C. Pereira, Preparation and characterization of Ti/RuO_2 anodes obtained by sol–gel and conventional routes, Mater. Lett. 53 (2002) 339–345.
[26] C.C. Hu, Y.H. Huang, K.H. Chang, Annealing effects on the physicochemical characteristics of hydrous ruthenium and ruthenium-iridium oxides for electrochemical supercapacitors, J. Power Sources 108 (2002) 117–127.
[27] L.A. Faria, J.F.C. Boodts, S. Trasatti, Physico-chenical and electrochemical characterization of Ru-based ternary oxides containing Ti and Ce, Electrochim. Acta 37 (1992) 2511–2518.
[28] L.A. Faria, J.F.C. Boodts, S. Trasatti, Electrocatalytic properties of ternary oxide mixtures of composition Ru0.3Ti(0.7−x)$CexO_2$: oxygen evolution from acidic solution, J. Appl. Electrochem. 26 (1996) 1195–1199.
[29] J.F.C. Boodts, L.M. Silva, L.A. Faria, 'In situ' and 'ex situ' characterization of the surface properties of the RuO2(x)+Co3O4(1-x) system, Electrochim. Acta 45 (2000) 2719–2727.
[30] M.C. Liu, L.B. Kong, C. Lu, X.M. Li, Y.C. Luo, L. Kang, Facile fabrication of $CoMoO_4$ nanorods as electrode material for electrochemical capacitors, Mater. Lett. 94 (2013) 197–200.
[31] W.G. Pell, B.E. Conway, Quantitative modeling of factors determining Ragone plots for batteries and electrochemical capacitors, J. Power Sources 63 (1996) 255–266.
[32] F. Béguin, E. Franckowiak, Supercapacitors: Materials, Systems, and Applications, Wiley-VCH, Germany, 2013, pp. 326–328.
[33] Ch Yang, Ch Ying, V. Li, F. Li, K. Chan, Complex impedance with transmission line model and complex capacitance analysis of ion transport and accumulation in hierarchical core-shell porous carbons, J. Electrochem. Soc. 160 (2013) H271–H278.
[34] V. Ganesh, S. Pitchumani, V. Lakshminarayanan, New symmetric and asymmetric supercapacitors based on high surface area porous nickel and activated carbon, J. Power Sources 158 (2006) 1523–1532.
[35] H. Randriamahazaka, K. Asaka, Electromechanical analysis by means of complex capacitance of bucky-gel actuators based on single-walled carbon nanotubes and an ionic liquid, J. Phys. Chem. C 114 (2010) 17982–17988.
[36] P.L. Taberna, P. Simon, J. Fauvarque, Electrochemical characteristics and impedance spectroscopy studies of carbon-carbon supercapacitors, J. Electrochem. Soc. 150 (2003) A292–A300.
[37] A. Oz, S. Hershkovitz, N. Belman, E.T. Gutelmacher, Y. Tsur, Analysis of impedance spectroscopy of aqueous supercapacitors by evolutionary programming: finding DFRT from complex capacitance, Solid State Ionics 288 (2016) 311–314.
[38] P.R. Deshmukh, S.N. Pusawale, C.D. Lokhande, Supercapacitive performance of hydrous ruthenium oxide (RuO2·nH2O) thin films synthesized by chemical route at low temperature, Bull. Mater. Sci. 36 (2013) 1171–1176.
[39] F.Ç. Cebeci, H. Geyik, E. Sezer, A.S. Sarac, Synthesis, electrochemical characterization and impedance studies on novel thiophene-nonylbithiazole-thiophene comonomer, J. Electroanal. Chem. 610 (2007) 113–121.